EDGE ARTICLE

Check for updates

Nanocluster growth *via* "graft-onto": effects on geometric structures and optical properties†

Xi Kang, ‡[ac] Shan Jin,‡[b] Lin Xiong,[d] Xiao Wei,[ac] Manman Zhou,[ac] Chenwanli Qin,[ac] Yong Pei,[d] Shuxin Wang *[ac] and Manzhou Zhu *[abc]

Atomically precise engineering on the nanocluster surface remains highly desirable for the fundamental understanding of how surface structures of a nanocluster contribute to its overall properties. In this paper, the concept of "graft-onto" has been exploited to facilitate nanocluster growth on surface structures. Specifically, the $Ag_2(DPPM)Cl_2$ complex is used for re-constructing the surface structure of $Pt_1Ag_{28}(SR)_{18}(PPh_3)_4$ (Pt_1Ag_{28}, SR = 1-adamantanethiolate) and producing a size-growth nanocluster – $Pt_1Ag_{31}(SR)_{16}(DPPM)_3Cl_3$ (Pt_1Ag_{31}). The grafting effect of $Ag_2(DPPM)Cl_2$ induces both direct changes on the surface structure (*e.g.*, size growth, structural transformation, and surface rotation) and indirect changes on the kernel structure (from a fcc configuration to an icosahedral configuration). Remarkable differences have been observed by comparing optical properties between Pt_1Ag_{28} and Pt_1Ag_{31}. Significantly, Pt_1Ag_{31} exhibits high photo-luminescent intensity with a quantum yield of 29.3%, which is six times that of the Pt_1Ag_{28}. Overall, this work presents a new approach (*i.e.*, graft-onto) for the precise dictation of nanocluster surface structures at the atomic level.

1 Introduction

It has long been nano-scientists' dream to control compositions and structures of nanomaterials at the atomic level. Through the continuous accumulation of synthetic experience and with the help of advanced analytical methods, researchers can now easily tailor the composition and the morphology of metal nanoparticles.[1,2] However, it still remains extremely difficult to realize the atomic-level tailoring of specific sites on the nanoparticle surface (for example, adding or deleting one or two metal atoms at a designated position), which is the most relevant to the physical–chemical properties of such nanomaterials.

Nanoclusters (so-called ultrasmall nanoparticles) are an emerging class of promising nanomaterials owing to their atomically precise structures and intriguing properties.[3,4] Because of the quantum size effect of nanoclusters, any perturbations on compositions/structures may induce tremendous variations on clusters' properties.[3–6] Knowledge and understanding of these structure–property correlations are keys to the ultimate goal in the nanocluster science – arbitrarily dictating the properties *via* precisely tailoring the structures. Exploring effective approaches to exquisitely tailor the size, structure, and composition of atomically precise nanoclusters is a prerequisite to achieve this goal.

In recent years, ligand engineering has served as an efficient approach to convert structures of nanoclusters.[7] In general, great structural transformation occurs when the peripheral ligands of nanoclusters are drastically substituted by the introduced ligands (for instance, from mono-icosahedral $Au_{11}(PPh_3)_3Cl_3$ to bi-icosahedral $Au_{25}(PPh_3)_{10}(SR)_5Cl_2$,[7a] from $Ag_{44}(SR)_{30}$ with a hollow kernel to $Ag_{25}(SR)_{18}$ with a nonhollow kernel,[7b] and so on). However, it still remains challenging to tailor specific sites on the nanocluster surface without constructing the overall structure. A new approach for tailoring the nanocluster surface is highly desirable for the fundamental understanding of how surface structures in a nanocluster contribute to its overall properties.

By noting two facts about nanoclusters that (i) it is hard to substitute thiol ligands on the nanocluster surface by the introduced phosphorus ligands (because the metal–S covalent bond is more robust than the metal–P coordination bond) and (ii) several thiolated nanoclusters are terminally capped by

a Department of Chemistry and Centre for Atomic Engineering of Advanced Materials, Anhui Province Key Laboratory of Chemistry for Inorganic/Organic Hybrid Functionalized Materials, Anhui University, Hefei, Anhui, 230601, P. R. China. E-mail: ixing@ahu.edu.cn; zmz@ahu.edu.cn

b Institutes of Physical Science and Information Technology, Anhui University, Hefei, Anhui 230601, P. R. China

c Key Laboratory of Structure and Functional Regulation of Hybrid Materials, Anhui University, Ministry of Education, Hefei, 230601, P. R. China

d Department of Chemistry, Key Laboratory of Environmentally Friendly Chemistry and Applications of Ministry of Education, Xiangtan University, Xiangtan, Hunan 411105, China

† Electronic supplementary information (ESI) available: Fig. S1–S14 and Tables S1–S3 for the EDS, ESI-MS, XPS, ICP, TGA, and stability and PL results of nanoclusters, and the structural comparison between nanoclusters. CCDC 1937755. For ESI and crystallographic data in CIF or other electronic format see DOI: 10.1039/c9sc05700e

‡ These authors contributed equally to this work.

metal–PPh$_3$ units (such as **Pt$_1$Ag$_{28}$**(SR)$_{18}$(PPh$_3$)$_4$, Ag$_{29}$(SSR)$_{12}$(PPh$_3$)$_4$, and Ag$_{33}$(SR)$_{24}$(PPh$_3$)$_4$ clusters with Ag–PPh$_3$ terminals),[8] we perceive a good opportunity to re-construct the nanocluster surface without largely affecting its whole structure – substituting these terminal metal–PPh$_3$ units by bidentate phosphorus metal complexes. Such a substitution may not only fine-tune the nanocluster surface structure, but also shed light on structure–property correlations at the atomic level.

In the current work, we report a "graft-onto" strategy to facilitate a controllable size-growth of the nanocluster surface. Induced by the addition of the Ag$_2$(DPPM)Cl$_2$ complex (DPPM = bis-(diphenylphosphino)-methane), **Pt$_1$Ag$_{28}$**(SR)$_{18}$(PPh$_3$)$_4$ (**Pt$_1$Ag$_{28}$**; SR = 1-adamantanethiolate) converts into a size-growth nanocluster – **Pt$_1$Ag$_{31}$**(SR)$_{16}$(DPPM)$_3$Cl$_3$ (**Pt$_1$Ag$_{31}$**). Great changes (including size growth, structural transformation, and surface rotation) take place on the outermost shell of **Pt$_1$Ag$_{28}$**, owing to the direct grafting effect of the Ag$_2$(DPPM)Cl$_2$. The changes on the outermost shell further induce the transformation of the innermost Pt$_1$Ag$_{12}$ kernel from a fcc configuration in **Pt$_1$Ag$_{28}$** to an icosahedral configuration in **Pt$_1$Ag$_{31}$**. **Pt$_1$Ag$_{28}$** and **Pt$_1$Ag$_{31}$** nanoclusters reflect remarkable differences in both optical absorption and PL emission. Significantly, **Pt$_1$Ag$_{31}$** displays high photo-luminescence (PL) intensity with a quantum yield (QY) of 29.3%, which is six times that of the **Pt$_1$Ag$_{28}$** (PL QY = 4.9%).

2 Experimental methods

Materials

All reagents were purchased from Acros Organics and Sigma-Aldrich and used without further purification: hexachloroplatinic(IV) acid (H$_2$PtCl$_6$·6H$_2$O, 99%, metals basis), silver nitrate (AgNO$_3$, 99% metals basis), adamantane-1-thiol (C$_{10}$H$_{15}$SH, HS-Adm, 95%), triphenylphosphine (PPh$_3$, 95%), bis(diphenylphosphino)methane ((C$_6$H$_5$)$_2$PCH$_2$P(C$_6$H$_5$)$_2$, DPPM, 98%), sodium borohydride (NaBH$_4$, 99.9%), sodium chloride (NaCl, 99.5%), sodium hexafluoroantimonate (NaSbF$_6$, 99%), rhodamine B (RB, for fluorescence), methylene chloride (CH$_2$Cl$_2$, HPLC, Aldrich), methanol (CH$_3$OH, HPLC, Aldrich), ethyl acetate (CH$_3$COOC$_2$H$_5$, HPLC, Aldrich), ethanol (CH$_3$CH$_2$OH, HPLC, Aldrich), ether (C$_2$H$_5$OC$_2$H$_5$, HPLC, Aldrich), and 2-methyltetrahydrofuran (C$_4$H$_7$O-2-CH$_3$, HPLC, Aldrich).

Synthesis of the [Pt$_1$Ag$_{28}$(S-Adm)$_{18}$(PPh$_3$)$_4$]Cl$_2$ nanocluster

For the nanocluster synthesis, AgNO$_3$ (29 mg, 0.17 mmol) and H$_2$PtCl$_6$·6H$_2$O (5 mg, 0.01 mmol) were dissolved in CH$_3$OH (5 mL) and CH$_3$COOC$_2$H$_5$ (35 mL). The solution was vigorously stirred (1200 rpm) with magnetic stirring for 15 min. Then, Adm-SH (0.1 g) and PPh$_3$ (0.1 g) were added and the reaction was vigorously stirred (1200 rpm) for another 90 min. After this, NaBH$_4$ aqueous solution (1 mL, 20 mg mL^{-1}) was added quickly to the above mixture. The reaction was allowed to proceed for 36 h under a N$_2$ atmosphere. After this, the aqueous layer was removed, and the mixture in the organic phase was rotavaporated under vacuum. Then approximately 30 × 3 mL of CH$_3$CH$_2$OH was used to wash the obtained nanoclusters. The precipitate was dissolved in CH$_2$Cl$_2$, which produced the

[**Pt$_1$Ag$_{28}$**(S-Adm)$_{18}$(PPh$_3$)$_4$]Cl$_2$ nanocluster. The yield is 45% based on the Ag element (calculated from AgNO$_3$) for the synthesis of [**Pt$_1$Ag$_{28}$**(S-Adm)$_{18}$(PPh$_3$)$_4$]Cl$_2$.

Synthesis of the Ag$_2$(DPPM)Cl$_2$ complex

0.17 g of AgNO$_3$ (1 mmol) was dissolved in 50 mL of CH$_3$CH$_2$OH, and NaCl aqueous solution (6 mL, 10 mg mL^{-1}) was added quickly to the above mixture. The reaction was stirred for 1 minute. The white precipitate was collected and rotavaporated under vacuum, which produced the AgCl powder. Then, 0.07 g of AgCl (0.5 mmol) was dispersed in 20 mL of CH$_2$Cl$_2$, to which solution 0.19 g DPPM was added. The reaction was vigorously stirred (1200 rpm) with magnetic stirring for 30 minutes. After this, the solution was evaporated to dryness, which produced the Ag$_2$(DPPM)Cl$_2$ complex. The yield is about 95% based on the Ag element (calculated from AgCl) for the synthesis of Ag$_2$(DPPM)Cl$_2$.

Synthesis of the [Pt$_1$Ag$_{31}$(S-Adm)$_{16}$(DPPM)$_3$Cl$_3$]Cl$_4$ nanocluster

For the nanocluster synthesis, 30 mg of [**Pt$_1$Ag$_{28}$**(S-Adm)$_{18}$(PPh$_3$)$_4$]Cl$_2$ was dissolved in 30 mL of CH$_2$Cl$_2$, to which 10 mg of Ag$_2$(DPPM)Cl$_2$ was added. The reaction was allowed to proceed for 10 minutes at room temperature. After this, the organic layer was separated from the precipitate and evaporated to dryness. Then, approximately 30 × 3 mL of CH$_3$CH$_2$OH was used to wash the obtained nanoclusters. The precipitate was dissolved in CH$_2$Cl$_2$, which produced the [**Pt$_1$Ag$_{31}$**(S-Adm)$_{16}$(DPPM)$_3$Cl$_3$]Cl$_4$ nanocluster. The yield is about 85% based on the Ag element (calculated from the **Pt$_1$Ag$_{28}$**) for the synthesis of [**Pt$_1$Ag$_{31}$**(S-Adm)$_{16}$(DPPM)$_3$Cl$_3$]Cl$_4$.

Single-crystal growth of [Pt$_1$Ag$_{31}$(S-Adm)$_{16}$(DPPM)$_3$Cl$_3$](SbF$_6$)$_4$

For accelerating the crystallization process and improving the quality of crystals, the counterion Cl$^-$ in [**Pt$_1$Ag$_{31}$**(S-Adm)$_{16}$(DPPM)$_3$Cl$_3$]Cl$_4$ was replaced by SbF$_6^-$. The reaction equation is [**Pt$_1$Ag$_{31}$**(S-Adm)$_{16}$(DPPM)$_3$Cl$_3$]Cl$_4$ + 4 SbF$_6^-$ → [**Pt$_1$Ag$_{31}$**(S-Adm)$_{16}$(DPPM)$_3$Cl$_3$](SbF$_6$)$_4$ + 4Cl$^-$. Specifically, 20 mg of [**Pt$_1$Ag$_{31}$**(S-Adm)$_{16}$(DPPM)$_3$Cl$_3$]Cl$_4$ was dissolved in 20 mL of CH$_2$Cl$_2$. Then, 1 mL of NaSbF$_6$–CH$_3$CH$_2$OH solution (5 mg mL^{-1}) was added. After 3 minutes, the organic layer was separated from the precipitate and evaporated to dryness. The precipitate was dissolved in CH$_2$Cl$_2$, which produced the [**Pt$_1$Ag$_{31}$**(S-Adm)$_{16}$(DPPM)$_3$Cl$_3$](SbF$_6$)$_4$ nanocluster. Nanoclusters were crystallized in a CH$_2$Cl$_2$/ether system with a vapor diffusion method. Specifically, 20 mg of clusters was dissolved in 5 mL of CH$_2$Cl$_2$, and the obtained solution was then vapor diffused using 50 mL of ether. After 3 days, dark red crystals of **Pt$_1$Ag$_{31}$** were collected and subjected to X-ray diffraction to determine the structure. The CCDC number of [**Pt$_1$Ag$_{31}$**(S-Adm)$_{16}$(DPPM)$_3$Cl$_3$](SbF$_6$)$_4$ is 1937755. Notably, the optical absorption and PL emission properties of the **Pt$_1$Ag$_{31}$** nanocluster remain unchanged after the counter-ion replacement.

Test of the temperature-photoluminescence (PL) intensity correlation

The nanocluster (0.1 mg) was dissolved in 5 mL of the CH$_2$Cl$_2$/C$_4$H$_7$O-2-CH$_3$ (v/v = 1 : 1) mixture. Then, the solutions were

cooled from 293 K to different temperatures and the PL spectra were measured.

X-ray crystallography

The data collection for single crystal X-ray diffraction was carried out on a Bruker Smart APEX II CCD diffractometer under a nitrogen flow at 170 K, using graphite-monochromatized Mo Kα radiation (λ = 0.71073 Å). Data reductions and absorption corrections were performed using the SAINT and SADABS programs, respectively.[9a] The electron density was squeezed using PLATON, and detailed information can be found in Table S3.† The structure was solved by direct methods and refined with full-matrix least squares on F^2 using the SHELXTL software package.[9b] All non-hydrogen atoms were refined anisotropically, and all the hydrogen atoms were set in geometrically calculated positions and refined isotropically using a riding model.

Theoretical methods

Density functional theory (DFT) calculations were employed to optimize the geometric structures and calculated the Kohn–Sham orbitals of $\mathbf{Pt_1Ag_{28}}$ and $\mathbf{Pt_1Ag_{31}}$ nanoclusters using the Perdew–Burke–Ernzerhof (PBE) GGA functional.[10a] The triple-zeta polarized (TZP) basis set with inclusion of the scalar relativistic effect *via* a zeroth-order regular approximation (ZORA) implemented in the ADF package was adopted.[10b]

Characterization

All UV-vis absorption spectra of the nanoclusters dissolved in CH_2Cl_2 were recorded using an Agilent 8453 diode array spectrometer, whose background correction was made using a CH_2Cl_2 blank.

Photo-luminescence (PL) spectra were measured on an FL-4500 spectrofluorometer with the same optical density (OD) of 0.05. In these experiments, the nanocluster solutions were prepared in CH_2Cl_2 at a concentration of less than 1 mg mL^{-1}.

Absolute quantum yield (QY) was measured with dilute solutions of nanoclusters on a HORIBA FluoroMax-4P. For determining the QYs of clusters, the nanocluster solutions were prepared in CH_2Cl_2 with the same OD of 0.05. Besides, the PL comparison between the $\mathbf{Pt_1Ag_{31}}$(S-Adm)$_{16}$(DPPM)$_3$Cl$_3$ nanocluster and rhodamine B was performed, to further determine the PL QY of the $\mathbf{Pt_1Ag_{31}}$(S-Adm)$_{16}$(DPPM)$_3$Cl$_3$ nanocluster.

Thermogravimetric analysis (TGA) was carried out on a thermogravimetric analyzer (DTG-60H, Shimadzu Instruments, Inc.). 10 mg of clusters was used for collecting the TGA data on clusters.

X-ray photoelectron spectroscopy (XPS) measurements were performed on a Thermo ESCALAB 250 configured with a monochromated Al Kα (1486.8 eV) 150 W X-ray source, 0.5 mm circular spot size, a flood gun to counter charging effects, and analysis chamber base pressure lower than 1×10^{-9} mbar.

Inductively coupled plasma-atomic emission spectrometry (ICP-AES) measurements were performed on an Atomscan advantage instrument from Thermo Jarrell Ash Corporation (USA).

Elemental analysis (EA) was performed on Vario EL cube. 3 mg of each cluster sample was used for collecting the EA data.

Energy-dispersive X-ray spectroscopy (EDS) analyses were performed on a JEOL JEM-2100F FEG TEM operated at 200 kV. Nanocluster powder samples were used for the analysis.

Electrospray ionization time-of-flight mass spectrometry (ESI-TOF-MS) measurements were performed using a MicrO-TOF-QIII high-resolution mass spectrometer; for preparing the ESI sample, the clusters were dissolved in CH_2Cl_2 (1 mg mL^{-1}) and diluted (v/v = 1 : 2) with methanol.

3 Results and discussion

$\mathbf{Pt_1Ag_{28}}$ was prepared first *via* an *in situ* synthetic procedure (see the Experimental section for more details). A combination of ESI-MS, UV-vis absorption, PL, XPS, ICP, and EA results unambiguously identified that the obtained $\mathbf{Pt_1Ag_{28}}$ nanocluster is the same as the one reported previously (Fig. S1, and Tables S1, S2†).[8h] The EDS results demonstrated the presence of Cl in the cluster system, which was considered as the counterion for the $\mathbf{Pt_1Ag_{28}}$ nanocluster, namely, $[\mathbf{Pt_1Ag_{28}}$(S-Adm)$_{18}$(PPh$_3$)$_4$]Cl$_2$ (Fig. S2†).

The reaction between $\mathbf{Pt_1Ag_{28}}$ and Ag$_2$(DPPM)Cl$_2$ generates a $\mathbf{Pt_1Ag_{31}}$ nanocluster, wherein the Ag–PPh$_3$ vertexes were substituted by the Ag$_2$(DPPM)Cl, accompanied by a size-growth of the metallic kernel from M$_{29}$ to M$_{32}$ (M = Pt/Ag; Fig. 1). As for the overall structure, the Ag–PPh$_3$ terminals (in $\mathbf{Pt_1Ag_{28}}$) are bonded onto the nanoclusters with an I-type growth mode, whereas the Ag$_2$(DPPM)Cl terminals (in $\mathbf{Pt_1Ag_{31}}$) follow a Y-type growth mode (Fig. 1). The transformation of the nanocluster terminal from the single-linked Ag–PPh$_3$ (I type; see Fig. 1A) into the double-linked Ag$_2$(DPPM)Cl (Y type; see Fig. 1B) reflects the "graft-onto growth" and accounts for the size growth, structural transformation, and surface rotation of the nanocluster.

The ESI-MS and EDS results identified the molecular formula as $[\mathbf{Pt_1Ag_{31}}$(S-Adm)$_{16}$(DPPM)$_3$Cl$_3$]Cl$_4$ (Fig. S3 and S4†). Both $\mathbf{Pt_1Ag_{28}}$ and $\mathbf{Pt_1Ag_{31}}$ clusters contain 8 free valence electrons – (i) for $\mathbf{Pt_1Ag_{28}}$, the free electron count is 28(Ag) − 18(SR) − 2(charge) = 8; (ii) for $\mathbf{Pt_1Ag_{31}}$, the free electron count is 31(Ag)
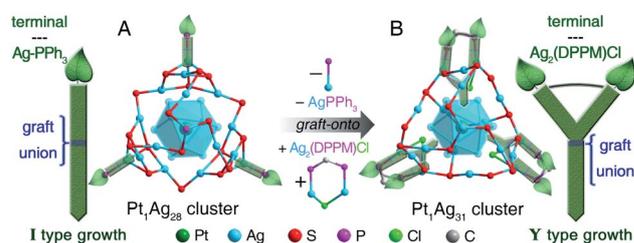
Fig. 1 Transformation from $\mathbf{Pt_1Ag_{28}}$ into $\mathbf{Pt_1Ag_{31}}$. (A) Schematic illustration of the I-type growth of the Ag−PPh$_3$ terminal and the structure of $\mathbf{Pt_1Ag_{28}}$. (B) Schematic illustration of the Y-type growth of the Ag$_2$(DPPM)Cl terminal and the structure of $\mathbf{Pt_1Ag_{31}}$. In this transformation process, the Ag−PPh$_3$ terminals in $\mathbf{Pt_1Ag_{28}}$ are peeled off, and the Ag$_2$(DPPM)Cl terminals are introduced. Color legends: dark green sphere, Pt; blue sphere, Ag; red sphere, S; purple sphere, P; green sphere, Cl; grey sphere, C. For clarity, all H atoms and some C atoms are omitted.

$- 16(SR) - 3 (Cl) - 4(charge) = 8$. The atomic ratio of Pt to Ag in **Pt$_1$Ag$_{31}$** was analyzed by XPS and ICP, and the experimental results were consistent with the theoretical ratio (Fig. S5, and Table S1†). TGA of the **Pt$_1$Ag$_{31}$** nanocluster showed a total weight loss of 52.65%, matching the theoretical value of 53.54% (the proportion of SR, DPPM, Cl ligands and the Cl counterion in the overall formula; Fig. S6†).

The structural comparison between **Pt$_1$Ag$_{28}$** and **Pt$_1$Ag$_{31}$** is shown in Fig. 2 (see Fig. S7† for the total structure of **Pt$_1$Ag$_{31}$**). **Pt$_1$Ag$_{28}$** comprises a fcc Pt$_1$Ag$_{12}$ kernel, a trilateral Ag$_{12}$(SR)$_{15}$(PPh$_3$)$_3$ shell, and a helical Ag$_4$(SR)$_3$(PPh$_3$)$_1$ unit (Fig. 2A–F). The trilateral Ag$_{12}$(SR)$_{15}$(PPh$_3$)$_3$ shell is constituted by assembling of three same Ag$_4$(SR)$_6$(PPh$_3$)$_1$ units (Ag$_3$(SR)$_6$ face + Ag–PPh$_3$ terminals) by sharing the terminal thiol ligands (Fig. 2B and M).

With the grafting effect, the vertex Ag-PPh$_3$ units on the **Pt$_1$Ag$_{28}$** surface are peeled off, and Ag$_2$(DPPM)Cl units are introduced. As a result, three additional Ag atoms (**Pt$_1$Ag$_{31}$** − **Pt$_1$Ag$_{28}$** = 3 Ag) are incorporated onto the nanocluster surface because of the grafting effect of bidentate DPPM ligands. Three Cl ligands are also introduced to further stabilize the surface structure of **Pt$_1$Ag$_{31}$**. More specifically—

(i) Although the composition of the Pt$_1$Ag$_{12}$ kernel maintains throughout the graft-onto process, the fcc configuration of the Pt$_1$Ag$_{12}$ kernel in **Pt$_1$Ag$_{28}$** alters to an icosahedral configuration in **Pt$_1$Ag$_{31}$** (Fig. 2A and G). The average bond length between Pt(core) and Ag(kernel surface) in **Pt$_1$Ag$_{31}$** is smaller than that in **Pt$_1$Ag$_{28}$**, whereas the bonds between Ag(kernel surface) and Ag(kernel surface) in **Pt$_1$Ag$_{31}$** are much longer than those in **Pt$_1$Ag$_{28}$** (Table 1 and Fig. S8†).

(ii) The trilateral Ag$_{15}$(SR)$_{13}$(DPPM)$_3$Cl$_3$ shell in **Pt$_1$Ag$_{31}$** is constituted by the assembly of three same Ag$_6$(SR)$_6$(DPPM)$_1$Cl$_1$ units *via* sharing Ag$_2$(SR)$_3$ edges (Fig. 2H and N). Due to the steric hindrance effect, only 13 thiol ligands exist in the trilateral Ag$_{15}$(SR)$_{13}$(DPPM)$_3$Cl$_3$ shell and less than the 15 thiol ligands in the Ag$_{12}$(SR)$_{15}$(PPh$_3$)$_3$ trilateral shell of **Pt$_1$Ag$_{28}$** (Fig. 2B and H). In each Ag$_6$(SR)$_6$(DPPM)$_1$Cl$_1$ unit, the Cl ligand fixes two Ag atoms that bond with the DPPM ligand (Fig. 2N). All Ag-ligand interactions (including Ag(kernel surface)–S(motif), Ag(motif)–S(motif), and Ag(motif)–P(vertex)) in **Pt$_1$Ag$_{31}$** are longer than those in **Pt$_1$Ag$_{28}$** (Table 1).

(iii) The Pt$_1$Ag$_{24}$(SR)$_{15}$(PPh$_3$)$_3$ structure in **Pt$_1$Ag$_{28}$** is covered by a helical Ag$_4$(SR)$_3$(PPh$_3$)$_1$ unit (Fig. 2D), whereas the corresponding structure in **Pt$_1$Ag$_{31}$** is just Ag$_4$(SR)$_3$ (Fig. 2J); that is, the terminal PPh$_3$ ligand is peeled off. A similar situation has recently been observed in the transformation of Ag$_{29}$(SSR)$_{12}$(PPh$_3$)$_4$ into Cs$_3$Ag$_{29}$(SSR)$_{12}$(DMF)$_x$.[11] For the Cs$_3$Ag$_{29}$(SSR)$_{12}$(DMF)$_x$ nanocluster, because of the absence of the vertex PPh$_3$ ligand, the terminal Ag atom becomes closer to the innermost Ag$_{13}$ kernel.[11] A similar situation has been observed in this work – the average distance between the terminal Ag and adjacent Ag atoms in the innermost Pt$_1$Ag$_{12}$ kernel in **Pt$_1$Ag$_{31}$** is 4.026 Å, which is much shorter than that in **Pt$_1$Ag$_{28}$** (4.290 Å, as shown in Fig. S9†). In this context, the terminal Ag-based structure in **Pt$_1$Ag$_{31}$** becomes more contractive for reducing the exposure of this bare Ag atom, which in turn makes the overall structure more robust.

Collectively, the "graft-onto" process on the **Pt$_1$Ag$_{28}$** surface changes the vertex structure from PPh$_3$-Ag to DPPM-Ag$_2$-Cl, resulting in the size-growth and surface structural
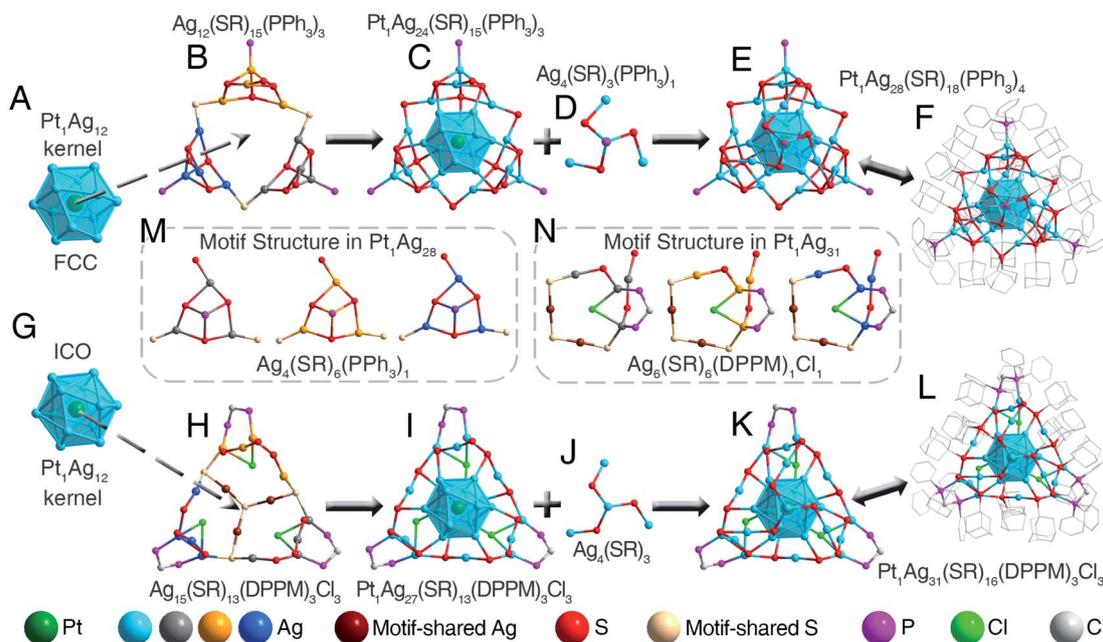

Fig. 2 Structural anatomies of **Pt$_1$Ag$_{28}$** and **Pt$_1$Ag$_{31}$** nanoclusters. (A–F and M) Structural anatomy of the **Pt$_1$Ag$_{28}$** nanocluster. (G–L and N) Structural anatomy of the **Pt$_1$Ag$_{31}$** nanocluster. Color legends: dark green sphere, Pt; blue/dark grey/orange/dark blue sphere, Ag; brown sphere, motif-shared Ag; red sphere, S; pink sphere, motif-shared S; purple sphere, P; green sphere, Cl; grey sphere, C. For clarity, all H atoms and some C atoms are omitted.

Table 1 Comparison of bond lengths in Pt_1Ag_{28} and Pt_1Ag_{31} nanoclusters. Such bonds are highlighted in Fig. S8

	Pt_1Ag_{28}	Pt_1Ag_{31}	Diff.
Pt(core)–Ag(kernel surface) bond	2.768–2.797 Å (Avg. 2.838 Å)	2.735–2.786 Å (Avg. 2.760 Å)	−2.83%
Ag(kernel surface)–Ag (kernel surface) bond	2.751–2.848 Å (Avg. 2.802 Å)	2.817–3.144 Å (Avg. 2.906 Å)	+3.58%
Ag(kernel surface)–S(motif) bond	2.438–2.498 Å (Avg. 2.472 Å)	2.445–2.591 Å (Avg. 2.495 Å)	+0.92%
Ag(motif)–S(motif) bond	2.254–2.992 Å (Avg. 2.560 Å)	2.356–2.835 Å (Avg. 2.460 Å)	+4.07%
Ag(motif)–P(vertex) bond	2.292–2.384 Å (Avg. 2.356 Å)	2.397–2.428 Å (Avg. 2.405 Å)	+2.04%

transformation of the nanocluster. The transformation of the outermost shell further induces changes on kernel–shell interactions, and such changes alter the innermost Pt_1Ag_{12} kernel from a fcc configuration in Pt_1Ag_{28} to an icosahedral configuration in Pt_1Ag_{31}.

From the structural point of view, aside from Pt_1Ag_{28}(-SR)$_{18}$(PPh$_3$)$_4$, several other metal nanoclusters are terminally capped by metal–PPh$_3$, such as Ag$_{29}$(SSR)$_{12}$(PPh$_3$)$_4$, Ag$_{33}$(SR)$_{24}$(-PPh$_3$)$_4$, Au$_{23}$(PhC≡C)$_9$(PPh$_3$)$_6$, Au$_{24}$(PhC≡C)$_{14}$(PR)$_4$, and so on.[8] Our reported "graft-onto" strategy might also be applicable in these cluster systems for controlling their surface structures. Future work will focus on extending the "graft-onto" strategy to other cluster systems.

Both Pt_1Ag_{28} and Pt_1Ag_{31} nanoclusters are stable in DMF at 50 °C for at least 24 hours (Fig. S10A and C†). At 80 °C, the optical absorptions of Pt_1Ag_{28} disappear over time (Fig. S10B†); by comparison, the Pt_1Ag_{31} nanocluster is stable enough to maintain its optical absorptions (Fig. S10D†). We propose that the enhanced thermal stability of Pt_1Ag_{31} results from its more robust structure – compared with PPh$_3$, the introduced DPPM ligands have more ability to fix the nanocluster surface and thus suppress the vibration of the overall structure.

The optical properties of Pt_1Ag_{28} and Pt_1Ag_{31} nanoclusters are compared. Optical absorption of Pt_1Ag_{28} shows an intense peak at 445 nm and a shoulder peak at 540 nm. The transformation of Pt_1Ag_{28} into Pt_1Ag_{31} results in an obvious blue-shift for each peak – the peak at 445 nm blue-shifts to 430 nm and becomes wider, and the shoulder band at 540 nm blue-shifts to 525 nm (Fig. 3A). The blue shift of the maximum optical absorption of nanoclusters (i.e., from 540 nm of Pt_1Ag_{28} to 525 nm of Pt_1Ag_{31}) always represents the enlargement of the HOMO–LUMO energy gap (HOMO: the highest occupied molecular orbital; LUMO: the lowest unoccupied molecular

orbital), which matches the DFT calculation results that Pt_1Ag_{31} displays a larger energy gap relative to Pt_1Ag_{28} (1.92 eV versus 1.76 eV, Fig. S11†).

The Pt_1Ag_{28} nanocluster (in CH$_2$Cl$_2$ solution) emits at 672 nm, with a photo-luminescence quantum yield (PL QY) of 4.9%.[8h] By comparison, the Pt_1Ag_{31} nanocluster (in CH$_2$Cl$_2$ solution, with the same OD as Pt_1Ag_{28} solution) emits at 651 nm, representing a 21 nm blue shift relative to that of the Pt_1Ag_{28}. Significantly, the PL QY of Pt_1Ag_{31} in CH$_2$Cl$_2$ is 29.3%; that is, the PL intensity of Pt_1Ag_{31} is six times that of the Pt_1Ag_{28}. Such an enhancement can also be inferred from the PL spectra of two nanoclusters (Fig. 3B). Besides, the PL comparison between Pt_1Ag_{31} and rhodamine B further determined the PL QY of the nanocluster (Fig. S12 and S13†). Under weak UV light, the emission of Pt_1Ag_{28} is hard to be observed, whereas the PL of Pt_1Ag_{31} is strong enough to be perceived with the naked eye (Fig. 3B, insets). Such a PL enhancement may result from the enhanced stabilization ability of DPPM relative to PPh$_3$ – the introduced DPPM ligand firmly fixes the surface structure and suppresses the vibration of the overall structure; in this context, the energy dissipation of the photo-excited Pt_1Ag_{31} reduces with non-radiative transitions (mainly affected by intramolecular vibrations), but enhances with radiative transitions (through luminescence).
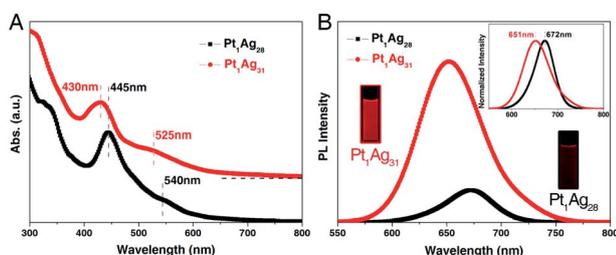

Fig. 4 Temperature-dependent PL of Pt_1Ag_{31} (dissolved in CH$_2$Cl$_2$). (A) Temperature-dependent emission of Pt_1Ag_{31}. (B) The PL intensity of Pt_1Ag_{31} at the fixed point of 651 nm. (C) The derivative results for the temperature-dependent PL intensity of Pt_1Ag_{31}. (D) Optical absorption of Pt_1Ag_{31} at 293 K and 179 K.

Fig. 3 Optical properties of nanoclusters. (A) Optical absorptions of Pt_1Ag_{28} and Pt_1Ag_{31} nanoclusters. (B) PL emissions of Pt_1Ag_{28} and Pt_1Ag_{31} nanoclusters. Insets in B: peak shift in normalized PL spectra, and digital photo of each cluster in CH$_2$Cl$_2$ under UV light.
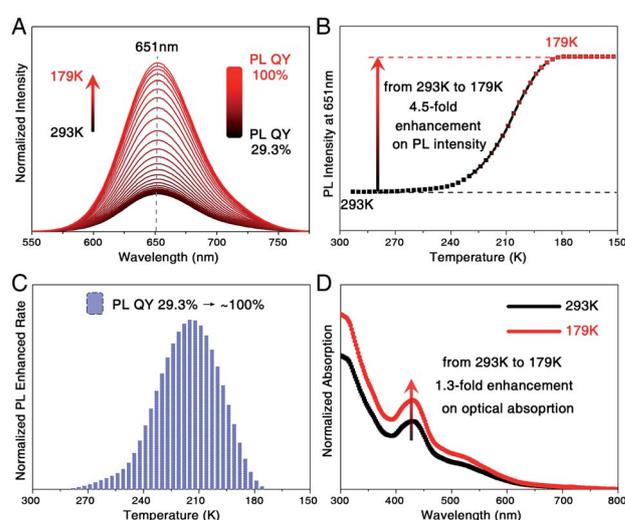
Temperature-dependent fluorescence of the **Pt₁Ag₃₁** nanocluster was monitored. For the **Pt₁Ag₂₈** nanocluster, our previous work demonstrated a 20-fold enhancement on the PL intensity of **Pt₁Ag₂₈** (in DMF solution) along with the temperature-lowering process from 293 K to 125 K, and the PL QY increased from 9.3% to ~100% (Fig. S14†).[12a] As to the **Pt₁Ag₃₁** nanocluster (Fig. 4), the PL intensity presented a 4.5-fold enhancement by comparing the 179 K data with the 293 K data (Fig. 4A–C), and the optical absorption just exhibited a 1.3-fold enhancement in the corresponding temperature-lowering process (Fig. 4D). Accordingly, the PL QY of **Pt₁Ag₃₁** was almost 100% when the temperature was lower than 179 K. Such an enhancement of PL intensity resulted from the reduced energy consumption of thermal vibrations of nanoclusters (non-radiative transition) reduced by the reduced temperature; in this context, the excitation energy could only be released by the PL approach (radiative transition).[11,12]

4 Conclusions

In summary, a "graft-onto" strategy is presented for facilitating a controllable size-growth of the nanocluster surface. The addition of the $Ag_2(DPPM)Cl_2$ complex converts **Pt₁Ag₂₈**(S-Adm)₁₈(PPh₃)₄ into a size-growth nanocluster, namely, **Pt₁Ag₃₁**(S-Adm)₁₆(DPPM)₃Cl₃. Induced by the grafting effect, direct changes on the surface structure (e.g., size growth, structural transformation, and surface rotation) and indirect changes on the kernel structure (from a fcc configuration to an icosahedral configuration) take place. Obvious differences have been observed by comparing the optical properties (optical absorption and PL emission) of two nanoclusters. Significantly, **Pt₁Ag₃₁**(SR)₁₆(DPPM)₃Cl₃ displayed a high PL intensity with a PL QY of 29.3%, which is six times that of the **Pt₁Ag₂₈**(SR)₁₈(PPh₃)₄. Our work presents a new strategy for controllably reconstructing the nanocluster surface at the atomic level, which hopefully sheds light on the fundamental understanding of how surface structures in a nanocluster contribute to its overall properties.

Conflicts of interest

There are no conflicts to declare.

Acknowledgements

Notes and references

1 (a) Y. Xia, Y. Xiong, B. Lim and S. E. Skrabalak, *Angew. Chem., Int. Ed.*, 2009, **48**, 60; (b) A. R. Tao, S. Habas and P. Yang, *Small*, 2008, **4**, 310; (c) M. Grzelczak, J. Pérez-Juste, P. Mulvaney and L. M. Liz-Marzán, *Chem. Soc. Rev.*, 2008, **37**, 1783.

2 (a) Y. Sun and Y. Xia, *Science*, 2002, **298**, 2176; (b) Y. Yao, Z. Huang, P. Xie, S. D. Lacey, R. J. Jacob, H. Xie, F. Chen, A. Nie, T. Pu, M. Rehwoldt, D. Yu, M. R. Zachariah, C. Wang, R. Shahbazian-Yassar, J. Li and L. Hu, *Science*, 2018, **259**, 1489; (c) P.-C. Chen, M. Liu, J. S. Du, B. Meckes, S. Wang, H. Lin, V. P. Dravid, C. Wolverton and C. A. Mirkin, *Science*, 2019, **363**, 959; (d) J. L. Fenton, B. C. Steimle and R. E. Schaak, *Science*, 2018, **360**, 513.

3 (a) R. Jin, C. Zeng, M. Zhou and Y. Chen, *Chem. Rev.*, 2016, **116**, 10346; (b) I. Chakraborty and T. Pradeep, *Chem. Rev.*, 2017, **117**, 8208; (c) Q. Yao, X. Yuan, T. Chen, D. T. Leong and J. Xie, *Adv. Mater.*, 2018, **30**, 1802751; (d) B. Bhattarai, Y. Zaker, A. Atnagulov, B. Yoon, U. Landman and T. P. Bigioni, *Acc. Chem. Res.*, 2018, **51**, 3104; (e) P. Liu, R. Qin, G. Fu and N. Zheng, *J. Am. Chem. Soc.*, 2017, **139**, 2122; (f) M. Agrachev, M. Ruzzi, A. Venzo and F. Maran, *Acc. Chem. Res.*, 2019, **52**, 44; (g) K. Kwak and D. Lee, *Acc. Chem. Res.*, 2019, **52**, 12; (h) B. Nieto-Ortega and T. Bürgi, *Acc. Chem. Res.*, 2018, **51**, 2811; (i) K. L. D. M. Weerawardene, H. Häkkinen and C. M. Aikens, *Annu. Rev. Phys. Chem.*, 2018, **69**, 205; (j) W. W. Xu, X. C. Zeng and Y. Gao, *Acc. Chem. Res.*, 2018, **51**, 2739; (k) Q. Tang, G. Hu, V. Fung and D.-e. Jiang, *Acc. Chem. Res.*, 2018, **51**, 2793; (l) N. A. Sakthivel and A. Dass, *Acc. Chem. Res.*, 2018, **51**, 1774; (m) Z. Lei, X.-K. Wan, S.-F. Yuan, Z.-J. Guan and Q.-M. Wang, *Acc. Chem. Res.*, 2018, **51**, 2465; (n) J. Yan, B. K. Teo and N. Zheng, *Acc. Chem. Res.*, 2018, **51**, 3084; (o) T. Zhao, P. J. Herbert, H. Zheng and K. L. Knappenberger, *Acc. Chem. Res.*, 2018, **51**, 1433; (p) P. Chakraborty, A. Nag, A. Chakraborty and T. Pradeep, *Acc. Chem. Res.*, 2019, **52**, 2; (q) X. Kang and M. Zhu, *Chem. Soc. Rev.*, 2019, **48**, 2422; (r) Y. Negishi, W. Kurashige, Y. Niihori and K. Nobusada, *Phys. Chem. Chem. Phys.*, 2013, **15**, 18736.

4 (a) P. D. Jadzinsky, G. Calero, C. J. Ackerson, B. A. David and R. D. Kornberg, *Science*, 2007, **318**, 430; (b) A. Desireddy, B. E. Conn, J. Guo, B. Yoon, R. N. Barnett, B. M. Monahan, K. Kirschbaum, W. P. Griffith, R. L. Whetten, U. Landman and T. P. Bigioni, *Nature*, 2013, **501**, 399; (c) S. Takano, H. Hirai, S. Muramatsu and T. Tsukuda, *J. Am. Chem. Soc.*, 2018, **140**, 12314; (d) T.-A. D. Nguyen, Z. R. Jones, B. R. Goldsmith, W. R. Buratto, G. Wu, S. L. Scott and T. W. Hayton, *J. Am. Chem. Soc.*, 2015, **137**, 13319; (e) S. Sharma, K. K. Chakrahari, J.-Y. Saillard and C. W. Liu, *Acc. Chem. Res.*, 2018, **51**, 2475; (f) S. Hossain, Y. Niihori, L. V. Nair, B. Kumar, W. Kurashige and Y. Negishi, *Acc. Chem. Res.*, 2018, **51**, 3114; (g) Z. Gan, N. Xia and Z. Wu, *Acc. Chem. Res.*, 2018, **51**, 2774; (h) B. Du, X. Jiang, A. Das, Q. Zhou, M. Yu, R. Jin and J. Zheng, *Nat. Nanotechnol.*, 2017, **12**, 1096; (i) M. Sugiuchi, Y. Shichibu and K. Konishi, *Angew. Chem., Int. Ed.*, 2018, **57**, 7855; (j) C. A. Hosier and C. J. Ackerson, *J. Am. Chem. Soc.*, 2019, **141**, 309; (k) Y. Lin, P. Charchar, A. J. Christofferson, M. R. Thomas, N. Todorova, M. M. Mazo, Q. Chen, J. Doutch, R. Richardson, I. Yarovsky and M. M. Stevens, *J. Am. Chem. Soc.*, 2018, **140**, 18217; (l) G. Panapitiya, G. Avendaño-Franco, P. Ren, X. Wen, Y. Li and J. P. Lewis, *J. Am. Chem.*

Soc., 2018, **140**, 17508; (*m*) R.-W. Huang, Y.-S. Wei, X.-Y. Dong, X.-H. Wu, C.-X. Du, S.-Q. Zang and T. C. W. Mak, *Nat. Chem.*, 2017, **9**, 689; (*n*) S. Kenzler, C. Schrenk and A. Schnepf, *Angew. Chem., Int. Ed.*, 2017, **56**, 393.

5 (*a*) M. S. Bootharaju, C. P. Joshi, M. R. Parida, O. F. Mohammed and O. M. Bakr, *Angew. Chem., Int. Ed.*, 2016, **55**, 922; (*b*) G. Soldan, M. A. Aljuhani, M. S. Bootharaju, L. G. AbdulHalim, M. R. Parida, A.-H. Emwas, O. F. Mohammed and O. M. Bakr, *Angew. Chem., Int. Ed.*, 2016, **55**, 5749; (*c*) H. Yang, Y. Wang, H. Huang, L. Gell, L. Lehtovaara, S. Malola, H. Häkkinen and N. Zheng, *Nat. Commun.*, 2013, **4**, 2422; (*d*) J. Yan, H. Su, H. Yang, S. Malola, S. Lin, H. Häkkinen and N. Zheng, *J. Am. Chem. Soc.*, 2015, **137**, 11880; (*e*) M. A. Tofanelli, T. W. Ni, B. D. Phillips and C. J. Ackerson, *Inorg. Chem.*, 2016, **55**, 999; (*f*) Y. Negishi, W. Kurashige, Y. Niihori, T. Iwasa and K. Nobusada, *Phys. Chem. Chem. Phys.*, 2010, **12**, 6219; (*g*) S. Xie, H. Tsunoyama, W. Kurashige, Y. Negishi and T. Tsukuda, *ACS Catal.*, 2012, **2**, 1519; (*h*) W.-T. Chang, P.-Y. Lee, J.-H. Liao, K. K. Chakrahari, S. Kahlal, Y.-C. Liu, M.-H. Chiang, J.-Y. Saillard and C. W. Liu, *Angew. Chem., Int. Ed.*, 2017, **56**, 10178; (*i*) S. Hossain, W. Kurashige, S. Wakayama, B. Kumar, L. V. Nair, Y. Niihori and Y. Negishi, *J. Phys. Chem. C*, 2016, **120**, 25861; (*j*) A. Ghosh, O. F. Mohammed and O. M. Bakr, *Acc. Chem. Res.*, 2018, **51**, 3094.

6 (*a*) N. A. Sakthivel, M. Stener, L. Sementa, A. Fortunelli, G. Ramakrishna and A. Dass, *J. Phys. Chem. Lett.*, 2018, **9**, 1295; (*b*) T. Higaki, M. Zhou, K. J. Lambright, K. Kirschbaum, M. Y. Sfeir and R. Jin, *J. Am. Chem. Soc.*, 2018, **140**, 5691; (*c*) Q. Yao, X. Yuan, V. Fung, Y. Yu, D. T. Leong, D.-e. Jiang and J. Xie, *Nat. Commun.*, 2017, **8**, 927.

7 (*a*) Y. Shichibu, Y. Negishi, T. Watanabe, N. K. Chaki, H. Kawaguchi and T. Tsukuda, *J. Phys. Chem. C*, 2007, **111**, 7845; (*b*) M. S. Bootharaju, C. P. Joshi, M. J. Alhilaly and O. M. Bakr, *Chem. Mater.*, 2016, **28**, 3292; (*c*) G. Deng, S. Malola, J. Yan, Y. Han, P. Yuan, C. Zhao, X. Yuan, S. Lin, Z. Tang, B. K. Teo, H. Häkkinen and N. Zheng, *Angew. Chem., Int. Ed.*, 2018, **57**, 3421; (*d*) T.-A. D. Nguyen, Z. R. Jones, D. F. Leto, G. Wu, S. L. Scott and T. W. Hayton,

Chem. Mater., 2016, **28**, 8385; (*e*) X. Kang, L. Xiong, S. Wang, Y. Pei and M. Zhu, *Inorg. Chem.*, 2018, **57**, 335; (*f*) Y. Chen, C. Liu, Q. Tang, C. Zeng, T. Higaki, A. Das, D.-e. Jiang, N. L. Rosi and R. Jin, *J. Am. Chem. Soc.*, 2016, **138**, 1482; (*g*) H. Dong, L. Liao and Z. Wu, *J. Phys. Chem. Lett.*, 2017, **8**, 5338.

8 (*a*) L. G. AbdulHalim, M. S. Bootharaju, Q. Tang, S. D. Gobbo, R. G. AbdulHalim, M. Eddaoudi, D.-e. Jiang and O. M. Bakr, *J. Am. Chem. Soc.*, 2015, **137**, 11970; (*b*) C. Liu, T. Li, H. Abroshan, Z. Li, C. Zhang, H. J. Kim, G. Li and R. Jin, *Nat. Commun.*, 2018, **9**, 744; (*c*) F. Tian and R. Chen, *J. Am. Chem. Soc.*, 2019, **141**, 7107; (*d*) H. Yang, J. Yan, Y. Wang, H. Su, L. Gell, X. Zhao, C. Xu, B. K. Teo, H. Häkkinen and N. Zheng, *J. Am. Chem. Soc.*, 2017, **139**, 31; (*e*) X. Yuan, C. Sun, X. Li, S. Malola, B. K. Teo, H. Häkkinen, L.-S. Zheng and N. Zheng, *J. Am. Chem. Soc.*, 2019, **141**, 11905; (*f*) M. Bodiuzzaman, A. Ghosh, K. S. Sugi, A. Nag, E. Khatun, B. Varghese, G. Paramasivam, S. Antharjanam, G. Natarajan and T. Pradeep, *Angew. Chem., Int. Ed.*, 2019, **58**, 189; (*g*) M. J. Alhilaly, M. S. Bootharaju, C. P. Joshi, T. M. Besong, A.-H. Emwas, R. Juarez-Mosqueda, S. Kaappa, S. Malola, K. Adil, A. Shkurenko, H. Häkkinen, M. Eddaoudi and O. M. Bakr, *J. Am. Chem. Soc.*, 2016, **138**, 14727; (*h*) X. Kang, M. Zhou, S. Wang, S. Jin, G. Sun, M. Zhu and R. Jin, *Chem. Sci.*, 2017, **8**, 2581; (*i*) X. Lin, C. Liu, K. Sun, R. Wu, X. Fu and J. Huang, *Nano Res.*, 2019, **12**, 309; (*j*) X.-K. Wan, S.-F. Yuan, Q. Tang, D.-e. Jiang and Q.-M. Wang, *Angew. Chem., Int. Ed.*, 2015, **54**, 5977; (*k*) X.-K. Wan, W. W. Xu, S.-F. Yuan, Y. Gao, X.-C. Zeng and Q.-M. Wang, *Angew. Chem., Int. Ed.*, 2015, **54**, 9683.

9 (*a*) G. M. Sheldrick, *SADABS*, University of Gottingen, Gottingen, Germany, 1996; (*b*) G. M. Sheldrick, *Acta Crystallogr., Sect. C: Struct. Chem.*, 2015, **71**, 3.

10 (*a*) J. P. Perdew, K. Burke and M. Ernzerhof, *Phys. Rev. Lett.*, 1996, **77**, 3865; (*b*) ADF 2010.01, SCM, *Theoretical Chemistry*, Vrije Universiteit, Amsterdam, The Netherlands, http://www.scm.com.

11 X. Wei, X. Kang, Q. Yuan, C. Qin, S. Jin, S. Wang and M. Zhu, *Chem. Mater.*, 2019, **31**, 4945.

12 (*a*) X. Kang, S. Wang and M. Zhu, *Chem. Sci.*, 2018, **9**, 3062; (*b*) X. Kang, L. Huang, W. Liu, L. Xiong, Y. Pei, Z. Sun, S. Wang, S. Wei and M. Zhu, *Chem. Sci.*, 2019, **10**, 8685.